RSC Advances

PAPER

View Article Online
View Journal | View Issue

Cite this: *RSC Adv.*, 2024, **14**, 3578

Green synthesis of carbon dots from fish scales for selective turn off–on detection of glutathione

Yi Zhang, Chunyu Lei, Ping Dong, Peiyang Fu, Yun Zhang and Ruifang Hua *

Carbon dots as fluorescent probes were fabricated using readily available grass carp fish scales as the carbon source *via* one-step synthesis based on a pyrolytic reaction. The as-prepared grass carp fish scale carbon dots (GF-CDs) exhibited good biocompatibility and excellent optical properties with a high fluorescence quantum yield of 23.8%. Glutathione (GSH) is an essential small tri-peptide molecule present in every body cell and plays a crucial role *in vivo* and performs a wide range of biological functions. Ag^+ can effectively quench the fluorescence of GF-CDs because of the electron transfer between GF-CDs and Ag^+; however, the addition of GSH can significantly increase GF-CD-Ag^+ fluorescence. Because of their combination with Ag^+ and GSH, GF-CDs show selective fluorescence recovery. GF-CDs can serve as fluorescent probes for GSH detection. This detection method covered a wide linear range (1.6–36.0 μg mL^{-1}) with the lowest detection limit of 0.77 μg mL^{-1} and manifested great advantages such as a short analysis time, good stability, repeatability, and ease of operation.

Received 1st November 2023
Accepted 3rd January 2024

DOI: 10.1039/d3ra07444g

rsc.li/rsc-advances

Introduction

Glutathione (GSH, Fig. 1) is an important small tripeptide composed of glycine, glutamic acid, and cysteine and is present in nearly all types cell. The thiol-containing GSH tripeptide is used for maintaining the normal function of the human immune system.[1] GSH has many biological functions such as antioxidation, detoxification, free-radical scavenging, immunity enhancing, anti-aging, and anticancer activities. The GSH content in cells is a crucial factor in the clinical diagnosis of disease conditions such as cancer and diabetes.[2] The thiol group of GSH shows essential reducing properties and therefore can be used as a reductant in the body to protect the sulfhydryl group of proteins or enzymes from oxidation. The content of GSH is adjusted by oxidized glutathione during a redox cycle where GSH is converted into oxidized glutathione under the action of H_2O_2 and glutathione peroxidase, and oxidized glutathione can be converted back into GSH by glutathione reductase. Furthermore, the thiol group of GSH is nucleophilic and can combine with drugs or carcinogens, thus preventing drugs or carcinogens from combining with DNA, RNA and proteins to avoid poisoning.[3–5] Because of the bioactivity of GSH, scientists have worked on methods for rapidly detecting GSH, which include high-performance liquid chromatography, capillary electrophoresis, and electrochemical detection.[6–8] However, a novel assay for the selective detection of GSH is not yet established.

Nanotechnology has been widely used, and its development has progressed dramatically.[9,10] Hence, the safety implementation of nanoscience must be gradually improved to benefit human health.[11] Research should be committed to developing an environmentally friendly platform for green nanotechnology. Biomass is an abundant, low-polluting resource containing various organic compounds that can be utilized as nanomaterial precursors.[12] Each year, fishery processing generates thousands of tons of fishery waste, which is a great concern. Fish scales are an excellent source of protein, calcium carbonate, chitin, vitamins, and amino acids and are novel precursors for carbonaceous materials with well-characterized fluorescence properties. Lu[13] directly used the natural primitive form of fish scales with rich micro/nano structures to conduct cell contact interaction studies, proving that the natural surface of biowastes can regulate cell behavior. Fluorescent carbon dots were synthesized through hydrothermal treatment of an easily available fish scale precursor and exhibited good fluorescence, thus enabling their application as viable fluorescent nanoprobes for the detection of pharmaceutical molecules.[14]

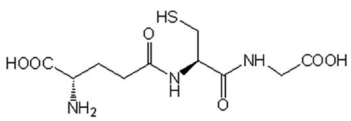

Fig. 1 Molecular structure of GSH.

Xinxiang Key Laboratory of Inflammation and Immunology, School of Medical Technology, Xinxiang Medical University, Xinxiang 453003, Henan, P. R. China. E-mail: huaruifang@xxmu.edu.cn; Fax: +86 373 3029977; Tel: +86 373 3029977

Carbon dots (CDs) are a type of novel carbon nanoparticle with sp^2 hybridized carbon nanostructures and an average particle size less than 10 nm.[15] CDs have superior luminescence and biocompatibility, making them attractive for biomarkers, nanoscale fluorescent probes, and biological imaging applications.[16–18] Because CDs contain many carboxylic acid moieties at their surface and can possess variable surface functionalities, microstructures, surface state, and crystalline state, they have a wide range of applications in addition to their use in sensing, drug delivery, environmental pollutant monitoring, diagnosis, and treatment of diseases.[19–21] Furthermore, the fast-growing synthetic route of CDs has provided numerous technological platforms for CD applications over the years. Low-cost CDs can be produced by a simple method through a one-step pathway and fast synthetic routes. Therefore, research and development of CDs with high performance and eco-friendly nature are crucial. Many CDs have already been produced with light stability, photoluminescence, and anti-photobleaching. CDs are proposed as a low-cost nanomaterial that can be used in drug detection applications as a safe alternative to organic dyes and semiconductor quantum dots.[22–24]

Biomass-derived carbon materials are the obvious choice for CDs because of their advantages of green economy and environmental protection.[25,26] Abundant organic matter contributes to the formation of nanoparticles coated with N-doped carbon during pyrolysis at high temperatures.[27,28] Fish scales are a kind of aquatic waste; each year, millions of tons of fish scales are produced worldwide.[29] Fish scales have a natural and unique structure and are an excellent source of carbon, nitrogen, and protein.[30] The richly structured surface of fish scales can benefit a broad range of applications.[31] The rational use of fish scales, skin, and other aquatic wastes can promote the sustainable development of aquatic processing and reduce environmental pollution.[32] We have used fish scales as the precursor for the preparation of nitrogen-doped CDs *via* simple hydrothermal treatment for the accurate fluorescence detection of lidocaine hydrochloride in 2018.[14] Crucian carp scale CDs were efficiently and selectively used for the quantitative detection of Fe^{3+} by us in 2019.[33] Considering that different precursors and biomass can be converted into CDs through controlled thermal treatment, fish scales was attempted as a precursor for the preparation of GF-CDs.

In the present work, grass carp fish scale carbon dots (GF-CDs) were fabricated through one-step pyrolysis of grass fish scales. Good biocompatibility is a prerequisite for applying GF-CDs to fluorescent probes or indicators. The cytotoxicity of GF-CDs was evaluated by a CCK-8 assay. Our results revealed that the GF-CDs demonstrated good biocompatibility and excellent fluorescence properties with a fluorescence quantum yield of 23.8%. We have previously prepared fish scale CDs, and the QY was not very high (less than 10%).[14] Ag^+ can quench the fluorescence of GF-CDs and the addition of GSH can increase GF-CDs-Ag^+ fluorescence. The GF-CDs can serve as fluorescent probes for GSH detection. Under optimum conditions, GSH was detected with high sensitivity, and the detection method covered a wide linear range (1.6–36.0 μg mL^{-1}) with a low detection limit of 0.77 μg mL^{-1}. The practical use of this GF-CD nanoprobe for GSH determination was also presented.

Experimental

Reagents

GSH was acquired from Sigma Aldrich. A stock solution of GSH at a concentration of 12.5×10^3 μg mL^{-1} was prepared and then kept at 4 °C in the darkness. Grass fish were bought from a local supermarket (Xinxiang, China). Common inorganic ion solutions such as $CaCl_2$, $ZnCl_2$ and NaCl as well as biological molecules such as amino acids were prepared using deionized water as the solvent. All other reagents were of analytical grade. A series of Britton–Robinson (BR) buffer solutions of pH in the range of 3–11 were prepared to evaluate the fluorescence feature under different media acidities. Deionized water was used for all experiments.

Preparation of GF-CDs

Grass carp was bought from a local aquaculture market (Xinxiang, China). We carefully scraped the scales off grass carp with knife and flushed them immediately with plenty of water. This step involves scrubbing off some bad fish scales and removing the dirt, mucus, and crud from the surface of them. The next step is to saturate the fish scales in a sodium hydroxide solution with a working mass concentration of one percent at room temperature for 24 h, which can allow the removal of proteins from the surface and avoid stinking. The fish scales were cleaned thoroughly with alcohol and then rinsed with water until the final pH value of the supernatant became neutral. Finally, the fish scales were dried and pulverized into a powder, which was subjected to a one-step pyrolytic route to obtain water-soluble GF-CDs. In brief, 1.0 g of fish scale powder was taken in a porcelain crucible and then transferred into a tube furnace for pyrolysis at 400 °C for 4.0 h in an Ar atmosphere. After cooling down naturally to room temperature, the black solid product obtained from the container was dissolved in water and centrifuged at 3000 rpm for 15 min to remove the sediment. GF-CD solutions were filtered through a 0.22 μm millipore cellulose membrane filter and then lyophilized, and the yield of GF-CDs was 4%. Stock solutions of GF-CDs with a concentration of 0.4×10^3 μg mL^{-1} were prepared for dilution treatment in the subsequent tests.

Characterizations

The morphology and particle size of GF-CDs were analyzed using a high-resolution transmission electron microscope (HRTEM, JEOL JEM 2100). X-ray powder diffraction patterns of GF-CDs were collected using a Bruker D8 X-ray diffractometer (Cu Kα radiation). The presence of various functional groups was identified using a Fourier transform infrared (FTIR) spectrometer (Thermo Nicolet FTS NEXUS; the sample was pressed in KBr pellets) in the range of 4000 to 400 cm^{-1}. X-ray photoelectron spectroscopy (XPS) analysis was carried out using an X-ray photoelectron spectrometer (ESCALAB250, Thermo, UK). UV-vis spectra (ultraviolet-visible) were recorded using a UV-

1700 UV spectrophotometer (Shimadzu, Kyoto, Japan). PL (photoluminescence) spectra were recorded using a FP-6500 instrument (Hitachi, Japan) with a 1 cm quartz cell. The relative fluorescence quantum yield of GF-CDs was determined based on the procedure reported in the literature.[34] A quinine sulfate solution (0.1 mol L^{-1}) was used as the reference (quantum yield was 54%). The fluorescence lifetimes of GF-CDs, GF-CDs-Ag^{+}, and GF-CDs-Ag^{+}-GSH in water were measured using a FlS-980 fluorescence spectrometer (Edinburgh Instrument, UK) with a 1 cm quartz cell respectively.

Cell toxicity

The degree of the absorbency was measured using an enzyme-labelling measuring instrument (Scientific Multiskan MK3 Enzyme Mark Instrument) to evaluate the cytotoxicity of GF-CDs on K562 cells (human leukemic cell line) by a cell counting kit-8 (CCK-8) assay (Beyotime, Shanghai, China).

Procedure for GSH detection

Unless specified otherwise, the primary test conditions of this developed "turn off–on" sensing platform for the determination of GSH are as follows: under optimum conditions, the GF-CDs were rapidly mixed with a given volume of Ag^{+} standard stock solution at a concentration of GSH of 1.6–36 μg mL^{-1}. The mixture CDs-Ag^{+}-GSH system had a constant GF-CD concentration of 20 μg mL^{-1}. After stirring at room temperature for 5 min, fluorescence emission spectra were gradually recorded with increasing concentrations of GSH at an excitation wavelength (λ_{ex}) of 400 nm with a slit width of 10 nm. The interference trials of inorganic ions and biomolecules were performed by monitoring the variation in the fluorescence emission intensities of CDs in the presence of these interferential substances.

Cell imaging

THP-1 cells (Human Monocyte Leukemia Cells, Tohoku Hospital Pediatrics-1) were cultured and maintained in a modified RPMI medium (Cytiva, USA). The media were supplemented with 5% fetal bovine serum (FBS) (Gibco, USA), and the THP-1 cells were maintained at 37 °C in a humidified atmosphere containing 5% CO_2. The THP-1 cells were incubated with GF-CDs, GF-CDs-Ag^{+}, and GF-CDs-Ag^{+}-GSH systems for 24 h. The fluorescence microscopic images were recorded using an inverted fluorescence microscope (Nikon Eclipse Ti-S) at different excitation wavelengths.

Results and discussion

Characterization of GF-CDs

GF-CDs can be obtained by one-step pyrolysis of grass fish scales at 400 °C in an Ar atmosphere for 4 h with bright blue fluorescence immediately under ultraviolet light irradiation, manifesting the fluorescence feature of GF-CDs. The synthesis procedure and schematic representation of how GF-CDs work for sensing GSH are presented in Fig. 2.

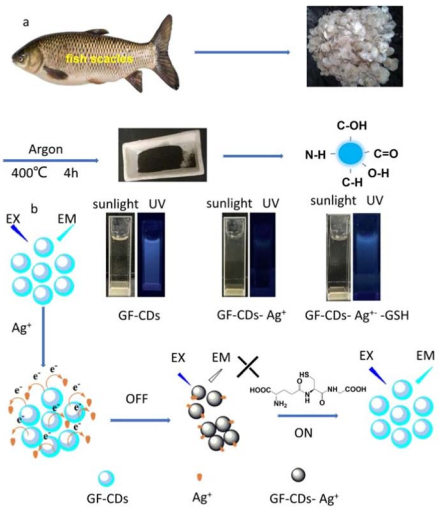

Fig. 2 (a) Illustration of the preparation of GF-CDs from fish scales. (b) Schematic diagram of the detection of GSH.

The TEM image of the afforded GF-CDs is shown in Fig. 3a. The HRTEM image (Fig. 3b) of GF-CDs displays well-ordered crystal lattice fringes with a spacing of 0.21 nm, which equivalents to the (100) facets of the aromatic carbon framework, indicating the formation of graphitic forms within the GF-CDs.[35] The range of the size distribution histogram (Fig. 3c) signifies the particles to be within 0.7–3.5 nm. The TEM images of the afforded GF-CDs-Ag^{+} and GF-CDs-Ag^{+}-GSH are presented in Fig. 3e and g. The ranges of the size distribution histogram

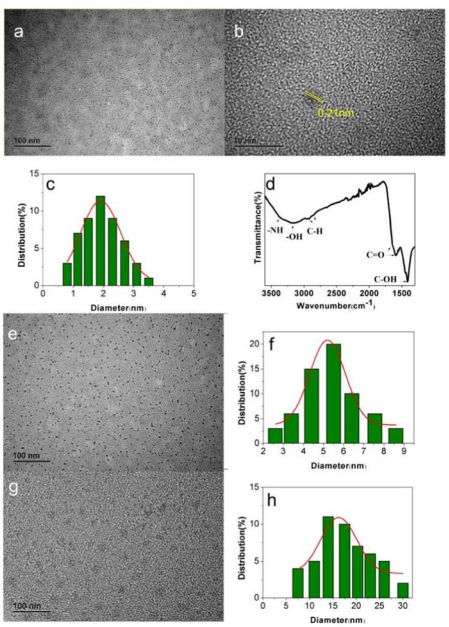

Fig. 3 (a) TEM image of GF-CDs. (b) HRTEM image of GF-CDs. (c) Associated particle size distribution of GF-CDs. (d) FTIR spectra of GF-CDs. (e) TEM image of GF-CDs-Ag^{+}. (f) Associated particle size distribution of GF-CDs-Ag^{+}. (g) TEM image of GF-CDs-Ag^{+}-GSH. (h) Associated particle size distribution of GF-CDs-Ag^{+}-GSH.

(Fig. 3f and h) signifies the size of the particles of GF-CDs-Ag^+ and GF-CDs-Ag^+-GSH systems to be within 2.6–8.6 nm and 7.5–30 nm. It has been proved that GF-CDs, Ag^+ and GSH can form a stable and uniform system under the studied concentration. Fourier transform infrared (FTIR) spectroscopy technique is commonly used to analyze the functional groups available on CDs. It is very common to find carboxylic and carbonyl functionalities from GF-CDs (Fig. 3d), as evident from the absorption peaks at 1638 cm^{-1} and 1608 cm^{-1}, which could be assigned to C=O.[31] The peaks at 3170 cm^{-1} and 3500 cm^{-1} were attributed to the stretching vibrations of –OH and –NH.[36] The small peaks at 2918 cm^{-1} and 2857 cm^{-1} were assigned to the vibration of –CH groups.[36] The absorption peaks at 1415 cm^{-1} could be assigned to N–H.[37] Generally, it can be concluded that the structure of GF-CDs indicates the presence of nitrogen-containing functional water groups and oxygen-containing functional groups with high content, which is beneficial for robust dispersion in aqueous solutions.

The surface chemical composition of GF-CDs was analyzed by XPS (Fig. 4). It can be seen from Fig. 4a that GF-CDs have three peaks at 285, 400, and 532 eV, corresponding to the spin orbital energies of C 1s, N 1s, and O 1s, respectively.[38] This indicates that the carbon groups in the material are enriched with C, N, and O elements. The percentage contents of carbon, nitrogen, and oxygen atoms are 53, 7.3, and 39, respectively. We fitted the C 1s, N 1s, and O 1s peaks of GF-CDs, and analyzed them in detail as follows: 284, 285, and 286 eV correspond to the bond energies of C=C/C–N, C–O, and C=O groups, respectively (Fig. 4b),[39] indicating the presence of O and N functional groups in GF-CDs. Fig. 4c shows the high-resolution N 1s spectrum, which can be divided into two peaks, corresponding to the bond energy of C–N–C (399.0 eV) and N–H (400.2 eV), indicating the effective binding of nitrogen to the carbon skeleton of GF-CDs. After fitting, the O 1s spectrum can be divided into two peaks (Fig. 4d), corresponding to the bond energies of C=O (531.2 eV) and C–OH (532.2 eV), respectively.[40,41] The XPS results of GF-CDs indicate that GF-CDs contain abundant O and N functional groups, which is consistent with the FTIR spectroscopy results. They provide necessary hydrophilicity and stability for GF-CDs as probes, and play a role in stabilizing chromogenic and assisting groups, thereby improving the practical application of GF-CDs.

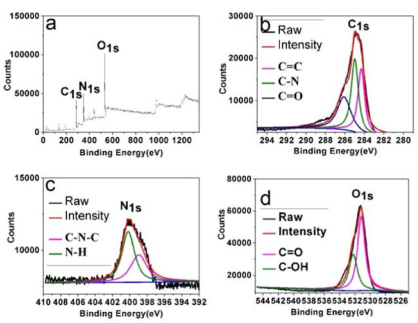

Fig. 4 (a) XPS survey spectra of GF-CDs. (b, c, and d) High-resolution XPS spectra of C 1s, N 1s, and O 1s peaks of GF-CDs.

The nitrogen doping of carbonaceous materials increases fluorescence by regulating the electronic properties and local chemical features of the carbon material.[42] The abundant nitrogen doping and high graphitization degree of the carbon matrix can effectively modulate the electronic states and transition channels. Thus, the fluorescence properties of CDs can be efficiently improved, and it is significant to develop techniques for the carbon matrix to play crucial roles in the fluorescent nanoprobe.[43]

Optical properties of GF-CDs

The fluorescence spectrum of the GF-CD solution at an excitation wavelength of 400 nm measured using a fluorospectrophotometer revealed that the GF-CD solution emitted strong fluorescence at 450 nm and showed the typical down-conversion fluorescence characteristics of GF-CDs (Fig. 5a); detecting the excitation spectrum of fluorescence revealed a solid excitation peak at 400 nm and a relatively feeble excitation peak intensity at 320 nm. Fig. 5b depicts the UV-visible absorption spectrum of GF-CDs in an aqueous solution, and GF-CDs exhibited strong absorption in the ultraviolet range of 270–400 nm and the characteristic absorption peak at 320 nm, which may be caused by the π–π* transition in the aromatic carbocycle skeleton and the n–π* transition in the C=O and C=N bonds.[44] Fig. 5c shows the fluorescence spectrum of the GF-CD aqueous solution at different excitation wavelengths. With the increase in excitation wavelength from 260 nm to 350 nm, the emission wavelength position of GF-CDs remains unchanged, and the emission intensity shows an increasing trend. The emission maximum shifts towards the red region while shifting the excitation wavelength from 360 to 450 nm, and the fluorescence intensity first increases and then decreases. The fluorescence emission of GF-CDs depends on excitation, indicating that GF-CDs have typical nanostructure characteristics.[45] A series of control experiments explored the optimal synthesis conditions of the grass carp scale precursor, such as different temperatures and reaction times, and considering quinine sulfate as the standard; the fluorescence quantum yield (QY) of GF-CDs was 23.8%. To further examine the cytotoxicity of GF-CDs, CCK-8 assays were performed using K-562 cells as the representative model. As shown in Fig. 5d,

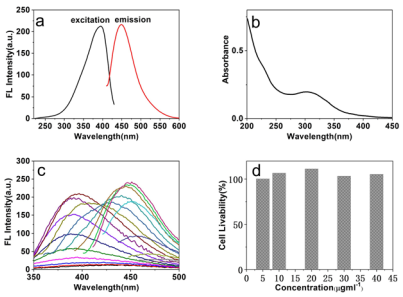

Fig. 5 (a) PL spectrum of GF-CDs. (b) UV-vis absorption spectrum of GF-CDs. (c) Fluorescence emission spectra of GF-CDs at excitation wavelengths of 260–450 nm. (d) Livability of K-562 cells incubated at different GF-CD concentrations.

over 98% of K-562 cells can still survive after incubation with GF-CDs in the concentration range of 5–40 μg mL^{-1} for 24 h. The high cell viability confirms negligible cytotoxicity and superior biocompatibility.

To further confirm the stability and dispersion of GF-CDs in aqueous solutions, we tested the fluorescence luminescence intensity of GF-CDs solutions of different concentrations (1.0–50 μg mL^{-1}). With the excitation wavelength at 400 nm, the fluorescence luminescence intensity of the GF-CDs aqueous solution increased with the concentration of GF-CDs (Fig. 6a), demonstrating the strong fluorescence, good dispersion, and stability of GF-CDs. The fluorescence spectrum of GF-CDs in the concentration range of this experiment had no self-quenching phenomenon, which makes GF-CDs fluorescent probes with excellent application potential in practical quantitative analysis. The GF-CDs showed good photostability when continuously irradiated with a xenon lamp of a fluorescence spectrophotometer for 2 h at an excitation wavelength of 400 nm. In addition, it was found that the NaCl solution at concentrations in the range of 0–25 mmol L^{-1} has influence on the fluorescence stability of GF-CDs, and the fluorescence intensity of GF-CDs was hardly changed, which is essential for the long-time detection of analytes in body fluids. Metal ions are widespread in a variety of different natural environment and can react with the surface functional groups of carbon dots, thus forming complexes and enhancing or decreasing the fluorescence intensity of CDs and changing the fluorescence property of CDs. Currently, there are some papers reporting that carbon dots can be used as fluorescent sensors to detect metal ions in actual samples.[46–48] The experiments on the impact of Ag^{+}, Au^{+}, Al^{3+}, Ba^{2+}, Co^{2+}, Ca^{2+}, Cd^{2+}, Cu^{2+}, Fe^{3+}, K^{+}, Mg^{2+}, Mn^{2+}, Na^{+}, Ni^{+}, Pb^{2+}, and Zn^{2+} (1.0 mmol L^{-1}) on the fluorescence property of GF-CDs have been researched. As shown in Fig. 6b and c, except for Au^{3+}, Co^{2+}, Cu^{2+}, and Fe^{3+}, which slightly quenched the fluorescence of GF-CDs in aqueous solutions, Ag^{+} significantly quenched the fluorescence intensity of GF-CDs. The addition of other metal ions had little effect on the fluorescence of GF-CDs, indicating that GF-CDs exhibited fluorescence response and good selectivity towards silver ions. The pH correlation of GF-CDs in the range of 3.0–11.0 was studied (Fig. 6d), and the fluorescence intensity of GF-CDs gradually increased in the pH range of 3.0–5.0. The fluorescence intensity of GF-CDs remains at a stable level within the pH range of 5.0 to 8.0. In the pH range of 8.0–11.0, the fluorescence intensity gradually decreased, and the emission wavelength slightly red-shifted. This pH-dependent PL feature may be caused by the protonation and deprotonation of GF-CDs surface functional groups. A physiological pH of 7.4 was chosen as the optimal environment for detecting GSH in the human body.

Fig. 7a depicts the dissolution of GF-CDs in different organic solvents under sunlight with good solubility. The color of GF-CDs in four solvents indicates that the solubility of GF-CDs increases with the increase in solvent dielectric constant. This phenomenon may be attributed to an increase in the dielectric constant of the solution, which enhances the binding ability of charges. For example, GF-CDs in an ethanol solvent show a very light-yellow color, whereas GF-CDs in a dimethyl formamide solvent show a dark brown color. Furthermore, insufficient pyrolysis of grass carp scales may result in the dissolution of some organic carbon-containing components that cannot emit light in organic solvents, thereby deepening the color of the solution. From Fig. 7b, it can be observed that under UV irradiation, GF-CDs solutions could emit bright blue fluorescence. The fluorescence quantum yield of GF-CDs in organic solvents was lower than that in water, which may be due to the absorption of carbon components that cannot emit light in the solution, reducing the fluorescence intensity. The influence of the organic solvents is negligible, as observed by comparing the experiments.

The absorption and fluorescence spectra of GF-CDs in acetone, ethanol, methanol, and dimethylformamide solvents were tested. Fig. 7 shows the fluorescence excitation and emission spectra of GF-CDs in acetone (Fig. 7c), ethanol

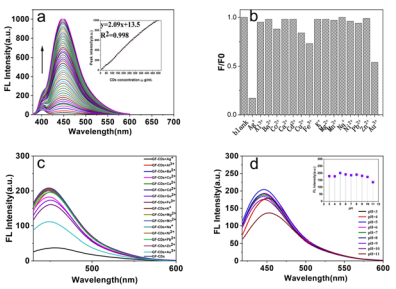

Fig. 6 (a) PL spectra of aqueous GF-CD solutions at different concentrations excited at 400 nm. (Inset) peak PL intensity as a function of GF-CD concentration. (b) PL intensity of the GF-CD solution in the presence of inorganic ions (1 mmol L^{-1}). (c) PL spectra of GF-CD interaction with metal ions. (d) PL spectra within the pH range 3–11. (Inset) PL intensity within the pH range 3–11.

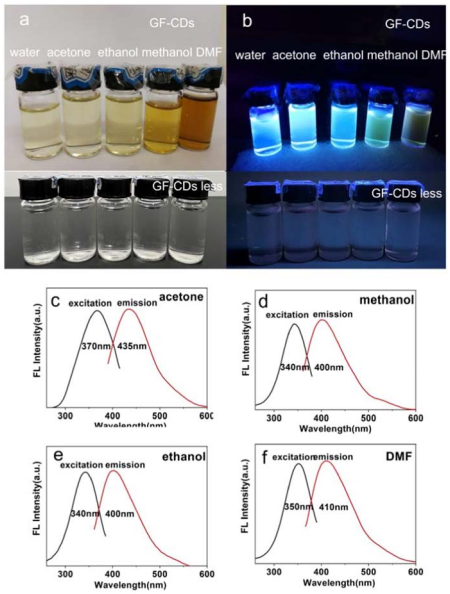

Fig. 7 (a) GF-CDs dissolved in different solvents. (b) GF-CDs dissolved in different solvents under UV irradiation. (c–f) PL spectra of GF-CDs dissolved in different solvents.

(Fig. 7d), methanol (Fig. 7e), and dimethylformamide (DMF) solvents (Fig. 7f). The findings indicate that GF-CDs exhibit different optical properties in different organic solvents. The absorption spectra of GF-CDs in ethanol and methanol with –OH groups had absorption peaks at 300 nm, whereas the excitation and emission peaks of the fluorescence spectra were at 340 nm and 400 nm, respectively. The UV absorption peak of GF-CDs shifted from 300 nm to 260 nm in acetone with the –C=O group, and the fluorescence excitation and emission peaks shifted from 370 nm to 435 nm. The absorption peak of GF-CDs shifted from 300 nm to 220 nm, and the fluorescence excitation and emission peaks red-shifted to 350 nm and 410 nm in DMF with the –S=O group. The –C=O group in acetone and the –S=O group in DMF were easy to interact with the π electrons in the graphite carbon structure in GF-CDs as electron acceptors, which sucks away the π electrons and change the optical characteristics of GF-CDs. The experiments on absorption and fluorescence detection of GF-CDs in different organic solvents can help us fully study the dissolution properties of GF-CDs, expanding the application area of GF-CDs.

Influence factor of optical properties and optimization of assay conditions

The pyrolysis temperature of the precursor had a significant effect on the optical properties of CDs.[49] The fluorescence and UV-visible absorption spectra of GF-CDs were tested at different temperatures. The experimental results indicated that the emission spectra of GF-CDs exhibited emission wavelength dependence with changes in excitation wavelength. As the pyrolysis temperature increased from 300 °C to 450 °C, the fluorescence intensity of GF-CDs increased, and the peak position remained unchanged. The UV-visible absorption peak of GF-CDs at 300 nm gradually increased. Furthermore, the fluorescence quantum yield of GF-CDs increased linearly with the increase in pyrolysis temperature. As shown in Fig. 8a, the fluorescence quantum yield of GF-CDs increased from 9.7% (300 °C) to 25% (450 °C). Considering factors such as over 400 °C and unstable performance of carbon materials, 400 °C was chosen as the optimal reaction temperature condition.

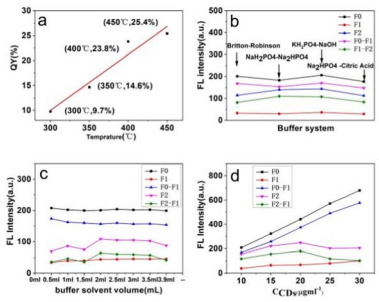

Fig. 8 (a) QY of GF-CDs prepared at 300, 350, 400, and 450 °C. Effect of (b) buffer solution type and (c) dosage of KH_2PO_4–NaOH buffer solution on the fluorescence intensity of the GF-CDs-Ag^+-GSH system. (d) Effect of GF-CD concentration on the PL intensity of the GF-CDs-Ag^+-GSH system.

The buffer solution plays a crucial role in maintaining a certain pH value of the system. The effects of adding 1.0 mL of different buffer solutions to the GF-CDs-Ag^+-GSH system were tested separately. As shown in Fig. 8b, the KH_2PO_4–NaOH buffer solution exhibited the strongest fluorescence intensity, indicating that the KH_2PO_4–NaOH buffer solution was the optimal buffer medium for detecting GSH in this experiment. To further understand the effect of the KH_2PO_4–NaOH buffer solution on the GF-CDs-Ag^+-GSH system, we measured the fluorescence intensity of the GF-CDs-Ag^+-GSH system at different dosages of KH_2PO_4–NaOH buffer solutions. As shown in Fig. 8c, the fluorescence intensity of the GF-CDs-Ag^+-GSH system did not change significantly when the KH_2PO_4–NaOH buffer solution was in the range of 0.5–3.9 mL. For 2.0 mL KH_2PO_4–NaOH buffer solution, the fluorescence intensity was significantly higher than that in other dosages. Approximately 2.0 mL of KH_2PO_4–NaOH buffer solution was the optimal dosage for this experiment.

To further optimize the reaction conditions of the GF-CDs-Ag^+-GSH system, we detected the influence of GF-CD concentrations on the fluorescence intensity of the GF-CDs-Ag^+-GSH system. The concentrations of Ag^+ and GSH were fixed at 0.010 mmol L^{-1} and 31 μg mL^{-1}, F_0 is the fluorescence intensity of GF-CDs, F_1 is the fluorescence intensity after addition of 0.010 mmol L^{-1} Ag^+, F_0–F_1 is the fluorescence intensity difference of GF-CDs quenched by silver ions, F_2 is the fluorescence intensity of the system after addition of 31 μg mL^{-1} GSH, and F_2–F_1 is the fluorescence intensity difference of the system recovered. Under no GSH added conditions, the fluorescence intensity increased linearly with the increase in GF-CD concentration (F_0). After the addition of silver ions into GF-CDs, the fluorescence intensity decreased (F_1). After the continuous addition of GSH, the fluorescence intensity increased (F_2), indicating that GSH could observably restore the fluorescence intensity of GF-CDs, and the fluorescence enhancement efficiency was also related to the concentration of GF-CDs (Fig. 8d). When the concentration of GF-CDs was 20 μg mL^{-1}, the fluorescence intensity amplitude of enhancement was greatest (F_2–F_1), possibly because the energy between GSH and Ag^+ transmitted more adequately at a GF-CD concentration of 20 μg mL^{-1}. Approximately 20 μg mL^{-1} was chosen as the optimal GF-CD concentration for detecting GSH.

The influence of Ag^+ concentration on the fluorescence intensity of the GF-CDs-Ag^+-GSH system was tested. F_0 was the fluorescence intensity when the GF-CD concentration was 20 μg mL^{-1}. F_1 was the fluorescence intensity after various Ag^+ concentrations were added. The fluorescence intensity of GF-CDs gradually decreased as the Ag^+ concentration increased until it stopped decreasing at an Ag^+ concentration of 50 × 10^{-3} mmol L^{-1}. F_0–F_1 was the fluorescence intensity difference of GF-CDs quenched by silver ions, and it changed slightly beyond an Ag^+ concentration of 50 × 10^{-3} mmol L^{-1}. F_2 was the fluorescence intensity of the system after addition of 16 μg mL^{-1} GSH, and F_2–F_1 was the fluorescence intensity difference of the system recovered. The fluorescence intensity of the system was increased after the addition of GSH (F_2), and the fluorescence enhancement efficiency was also related to the

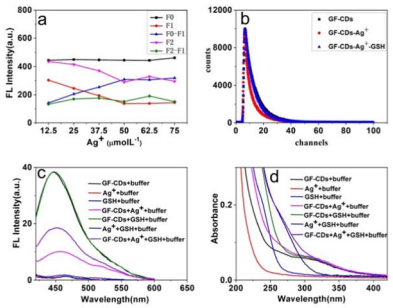

Fig. 9 (a) Effect of the Ag^+ concentration on the PL intensity of the GF-CD-Ag^+-GSH system. (b) Fluorescence decay curve of the aqueous GF-CD-Ag^+-GSH system solution. (c) Fluorescence spectra and (d) UV-vis absorption spectra of the GF-CD-Ag^+-GSH system.

concentration of Ag^+. As shown in Fig. 9a, when the concentration of Ag^+ was 62×10^{-3} mmol L^{-1}, the fluorescence intensity amplitude of enhancement was greatest (F_2–F_1). For the detection of GSH, 62×10^{-3} mmol L^{-1} was chosen as the optimal Ag^+ concentration.

The fluorescence lifetime of the GF-CDs-Ag^+-GSH system was further measured, as shown in Fig. 9b. The fluorescence lifetime of GF-CDs comprised two parts: 5.4 ns (42%) and 10 ns (58%). Through comparison and calculation, the average fluorescence lifetime of GF-CDs was 8.1 ns. After the addition of Ag^+, the fluorescence lifetime comprised 1.4 ns (9.3%), 4.7 ns (51%), and 13 ns (40%), and the lifetime decreased to 7.6 ns. After the addition of GSH, the fluorescence lifetime of the system was 5.4 ns (53%) and 9.6 ns (47%). The average fluorescence lifetime of the system was 7.4 ns, and the average fluorescence lifetime of the system remained almost unchanged. The addition of GSH almost completely overlapped with the fluorescence decay trend of the initial GF-CD solution, indicating that the possible reaction mechanism of the system could be that the fluorescence quenching of GF-CDs by Ag^+ belonged to static quenching.[50]

The feasibility of the GF-CDs-Ag^+-GSH system was evaluated using the fluorescence spectroscopy test. As shown in Fig. 9c, when the excitation wavelength was 400 nm, Ag^+, GSH and Ag^+-GSH solutions had almost no fluorescence, but the GF-CD solution exhibited strong fluorescence. The fluorescence intensity of the solution exhibited almost no change after the addition of GSH into the GF-CD solution, indicating no interaction between GF-CDs and GSH. By contrast, the fluorescence intensity of the GF-CD solution decreased when Ag^+ was added, confirming that Ag^+ could quench the fluorescence intensity of GF-CDs. The addition of GSH restored the fluorescence intensity of the GF-CDs-Ag^+ solution to a certain extent.

To explore the mechanism of the GF-CDs-Ag^+-GSH system, we scanned the absorption spectrum of the system. Fig. 9d shows that GF-CDs had an absorption peak at 300 nm, Ag^+ and GSH had almost no absorption at 300 nm, and the absorption spectrum of the Ag^+-GSH solution red-shifted and its absorption enhanced in the range of 260–350 nm, indicating a strong interaction between Ag^+ and GSH. After the addition of Ag^+ and GSH into the GF-CD solution, its final absorption spectrum was the sum of Ag^+ and GSH. The absorption spectrum of the GF-CDs-Ag^+-GSH solution was also obviously enhanced in the range of 260–350 nm. The possible reaction mechanism of the GF-CDs-Ag^+-GSH system could be that the excited GF-CDs transferred electrons to the d orbital of Ag^+ and formed the complex of GF-CDs-Ag^+, thus quenching the fluorescence of GF-CDs. After the addition of GSH to the GF-CDs-Ag^+ solution, GSH and Ag^+ formed an Ag–S bond, leading to the dissociation of the GF-CDs-Ag^+ complex; thus, the fluorescence of GF-CDs was restored. A dynamic equilibrium process would exist among GF-CDs, Ag^+ and GSH. The addition of GSH restored the fluorescence intensity of the GF-CDs-Ag^+ solution to a certain extent.

Fig. 10 shows the three-dimensional fluorescence spectra (Fig. 10a) and contour plots (Fig. 10b) of GF-CDs, GF-CDs-Ag^+, and GF-CDs-Ag^+-GSH systems. After the addition of Ag^+, the three-dimensional fluorescence spectrum of GF-CDs changed. From the intensity of the peak, the relative intensity of the fluorescence peak of GF-CDs was decreased. From the position of the peak, there was no significant change in the starting position of the fluorescence peak, and the corresponding contour stripes became significantly sparse. After the addition of GSH to the system, the peak intensity of the three-dimensional fluorescence spectrum of the system rebounded, and its contour lines became significantly denser. This result indicated that the interaction between GF-CDs and Ag^+ led to fluorescence quenching, whereas GSH combined with Ag^+ caused the fluorescence recovery of GF-CDs. Notably, a clear peak coordinate (E_X: 400 nm, E_M: 450 nm) was observed on the contour spectrum of GF-CDs, but no obvious absorption peak was found at 400 nm in the UV-visible absorption spectrum of GF-CDs. The absorption peak at 400 nm may be masked by strong absorption in the UV band. It was challenging to find a clear fluorescence peak from the three-dimensional fluorescence map because the 400 nm fluorescence emission peak's position was masked by the 450 nm fluorescence emission peak.

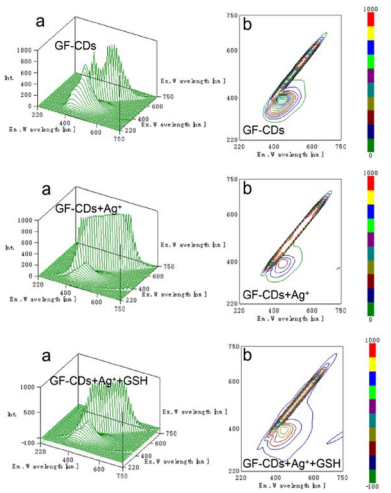

Fig. 10 (a) Three-dimensional PL spectra and (b) excitation–emission matrix (EEM) fluorescence spectra of GF-CDs-Ag^+-GSH.

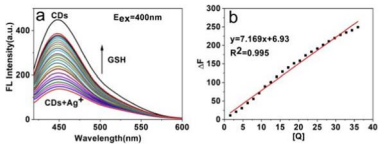

Fig. 11 (a) Fluorescence spectra of the GF-CDs-Ag^+-GSH system at different GSH concentrations. (b) Linear relationship between ΔF and GSH concentration.

Calibration curve and detection limit

The electrostatic interaction between Ag^+ and GF-CDs led to the fluorescence quenching of GF-CDs, producing non-fluorescent GF-CDs-Ag^+ complexes (turn-off). Further, the fluorescence intensity of GF-CDs-Ag^+ system was recovered with the increase of glutathione (GSH) by the Ag^+–S bonds between the coordinate GSH and Ag^+. With the increasing additives of GSH, Ag^+ combined with GSH rather than with GF-CDs and led to the removal of Ag^+ from the surface of GF-CDs and the gradual recovery of GF-CD fluorescence intensity (turn-on).[51–53] The fluorescence emission spectra of GF-CDs-Ag^+ at different GSH concentrations are shown in Fig. 11a under optimum conditions. Upon excitation at 400 nm, the emission intensity increased based on the concentration of GSH, demonstrating effective fluorescence enhancement of GF-CDs-Ag^+. From Fig. 11b, it can be observed that the fluorescence emission intensity of the GF-CDs-Ag^+ system increased monotonously with the increase in GSH concentration up to 36 μg mL^{-1}. The emission intensity of the GF-CDs-Ag^+-GSH system exhibited good linearity within the GSH concentration range of 1.6–36 μg mL^{-1}. The regression equation was $\Delta F = 7.2[Q] + 6.9$ (μg mL^{-1}), the correlation coefficient was 0.995 ($n = 23$), and the detection limit was 0.77 μg mL^{-1}, corresponding to the traditional counterparts[54–57] and implying that GF-CDs could serve as credible fluorescent nanoprobes for the quantitative detection of GSH. The GF-CDs-Ag^+-GSH system was tested 11 times in parallel, and a relative standard deviation of 0.46% ensured good reproducibility of GF-CD nanoprobes used for actual GSH analysis and detection. GSH significantly increased the intrinsic fluorescence of GF-CDs without changing the maximum emission wavelength. The effective synergistic effect indicates that GF-CDs have good application prospects as fluorescent probes for the quantitative detection of GSH.

To evaluate the specificity of this experimental method, we conducted interference experiments on amino acids and other related components. As shown in Table 1, in the GF-CDs-Ag^+-GSH system, although the concentration of other coexisting substances was twice that of GSH, they did not cause significant interference in the detection of GSH. The results indicated that the biomass GF-CDs derived from grass fish scales had sufficient anti-interference ability, could withstand interference from various external components and maintained good stability and specificity, which have practical application values for detecting GSH.

Detection of GSH in serum samples

To verify that this experimental method could detect the GSH content in actual samples, we analyzed and measured the GSH content in various higher animal serum samples using GF-CDs. The serum samples were centrifuged at 10 000 rpm, and their supernatant was obtained for storage and use. From Table 2, it can be found that the recovery rate detected in the sample was 93–102%, with a relative standard deviation of no more than 3.1%. These findings indicate that this experimental method is suitable for determining the GSH content in actual samples.

Table 1 Effects of potentially interfering substances on the GF-CD-Ag^+-GSH system

Foreign substances	Concentration (mmol L^{-1})	Recovery (%)	RSD (%, $n = 6$)
Starch	1	101	0.39
Fructose	1	101	0.37
DL-aspartic	1	102	0.61
L-lysine	1	101	0.40
Tryptophan	1	101	0.56
DL-leucine	1	102	0.87
L-arginine	1	101	0.65
L-methionine	1	101	0.46
DL-threonine	1	102	0.37
Glycine	1	102	1.0
DL-methionine	1	102	0.74
DL-proline	1	101	0.54
DL-lysine	1	102	1.2
Phenylalanine	1	102	0.34
Arginine	1	102	0.26
L-Leucine	1	101	0.94
Tyrosin	1	101	0.46

Imaging in cells

Given the robust fluorescence feature with low cytotoxicity, the capability of GF-CDs to transfer into cell was examined using

Table 2 GSH assay in different medium

Analyte	Medium	GSH concentration (μg mL^{-1}) Added	Found	Recovery (%)	RSD (%, $n = 6$)
		19	18	99	−2.9
GSH	Human serum1	22	20	93	2.5
		25	25	99	2.2
		19	19	101	3.1
GSH	Human serum2	22	22	100	2.4
		25	25	100	2.3
		19	19	102	0.50
GSH	Human serum3	22	22	102	0.60
		25	25	101	0.90
		19	19	102	0.6
GSH	Bovine serum	22	22	101	1.4
		25	25	100	1.1
		19	19	102	0.4
GSH	Rat serum	22	22	101	0.7
		25	25	101	0.4
		19	19	102	0.6
GSH	Rabbit serum	22	22	102	0.9
		25	25	101	0.9

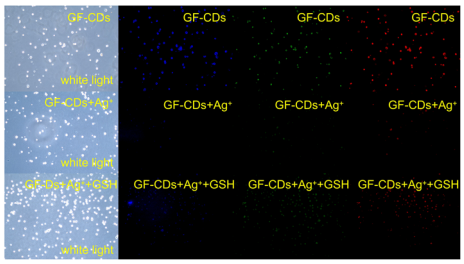

Fig. 12 Images of THP-1 cells after treatment with GF-CDs.

a fluorescence microscope at different excitation wavelengths. THP-1 cells were attempted as the model to assess the feasibility of the GF-CDs for intracellular bioimaging. Fig. 12 shows the white light and fluorescence microscopic images of GF-CDs, GF-CDs-Ag^+, and GF-CDs-Ag^+-GSH systems dyed THP-1 cells. Relative to the white light image, blue, green and red fluorescence were observable in the intracellular region of the THP-1 cells. After the addition of Ag^+, the imaging luminance of GF-CDs was decreased. The fluorescence intensity of the system rebounded with the addition of GSH. This outcome indicated the decrease in the fluorescence of the reaction GF-CDs with Ag^+, whereas GSH combined with Ag^+ causes fluorescence recovery. The fluorescence microscopic images demonstrated that GF-CDs can successfully transfer into THP-1 cells. Hence, the GF-CDs can be used as optical labels for *in vitro* cell imaging to deepen our understanding of the internalization mechanism of GF-CDs into cells, widening the application range of GF-CDs.

Conclusions

In summary, we adopted a simple and feasible one-step method to prepare GF-CDs with fluorescence characteristics from an environmentally friendly biomass carbon source (grass fish scales) without using any acids, bases, organic solvents, or metal ions. GF-CDs prepared *via* high-temperature pyrolysis exhibited high fluorescence quantum yields, good water solubility, wavelength-tunable properties and photostability and were expected to be used as nano fluorescent probes with excellent performance. Fluorescence spectrum testing revealed that GF-CDs exhibited strong emission spectra at 450 nm at an excitation wavelength of 400 nm. There was a strong electrostatic interaction and electron transfer between GF-CDs and Ag^+. Ag^+ could effectively quench the fluorescence of GF-CDs, and the fluorescence performance of GF-CDs was restored when GSH was added, which can be used to rapidly determine GSH. The synthesized GF-CDs were demonstrated to have good biocompatibility through cell survival rate.

Author contributions

Yi Zhang: conceptualization, methodology, investigation, writing original draft, funding acquisition. Chunyu Lei: investigation, data curation. Ping Dong: methodology, data curation. Peiyang Fu: investigation, data curation. Yun Zhang: project administration, supervision, funding acquisition. Ruifang Hua: writing – review & editing, project administration, supervision, funding acquisition.

Conflicts of interest

There are not conflicts to declare.

Acknowledgements

This work was supported by Key Scientific Research Projects of Key Scientific and Technological Projects of Henan Province (No. 222102310476 and 222102310310), Higher Education Institutions in Henan Province (No. 20B150020 and 23A330004), the National Natural Science Foundation of China (No. 32000708).

References

1 X. Z. Bao, X. H. Cao, K. L. Ai, Y. Cui, Z. G. Han, B. Zhou and C. D. Huo, *Sens. Actuators, B*, 2023, **382**, 133563.
2 W. Lu, S. H. Bao, H. F. Zhang, J. J. Qiu and X. Y. Liu, *J. Materiomics*, 2022, **8**(6), 1251–1259.
3 R. J. Mayer and A. R. Ofial, *Angew. Chem., Int. Ed. Engl.*, 2019, **58**(49), 17704–17708.
4 Y. Wang, F. S. Yen, X. G. Zhu, R. C. Timson, R. Weber, C. Xing, Y. Liu, B. Allwein, H. Luo, H. W. Yeh, S. Heissel, G. Unlu, E. R. Gamazon, M. G. Kharas, R. Hite and K. Birsoy, *Nature*, 2021, **599**(7883), 136–140.
5 M. K. Park, B. Y. Choi, A. R. Kho, S. H. Lee, D. K. Hong, B. S. Kang, S. H. Lee and S. W. Suh, *Int. J. Mol. Sci.*, 2023, **24**(3), 2950.
6 M. A. Khalikova, D. Satinsky, P. Solich, A. A. Zinchenko, E. T. Zhilyakovac and O. O. Novikov, *Anal. Methods*, 2014, **6**(5), 1475–1481.
7 D. Luo, Z. H. Fang, X. S. Zhao, Y. L. Ma, J. N. Ye and Q. C. Chu, *Electrophoresis*, 2019, **41**, 5–6.
8 S. A. B. Chotoye, M. M. Eisnor, R. B. E. Ball and C. L. Brosseau, *J. Raman Spectrosc.*, 2023, **54**(6), 587–595.
9 H. Hajiali, L. Ouyang, V. Llopis-Hernandez, O. Dobre and F. R. A. J. Rose, *Nanoscale*, 2021, **13**(23), 10266–10280.
10 F. Mascarenhas-Melo, M. B. S. Goncalves, D. Peixoto, K. D. Pawar, V. Bell, V. P. Chavda, H. Zafar, F. Raza and A. C. Paiva-Santos, *J. Drug. Target.*, 2022, **30**(10), 1034–1054.
11 A. Huguet-Casquero, E. Gainza and J. L. Pedraz, *Biotechnol. Adv.*, 2020, **46**(4), 107657.
12 L. K. Shrestha, R. G. Shrestha, S. Shahi, C. L. Gnawali, M. P. Adhikari, B. N. Bhadra and K. Ariga, *J. Oleo Sci.*, 2023, **72**(1), 11–32.
13 J. Y. Lu, F. R. Zhang, X. Z. Ding, L. Q. Xia and W. T. Huang, *Appl. Surf. Sci.*, 2022, **581**, 152348.
14 Y. Zhang, Z. Y. Gao, W. Q. Zhang, W. Wang, J. L. Chang and K. Jiang, *Sens. Actuators, B*, 2018, **262**, 928–937.
15 M. Perikala, R. Valoor, N. Bhaskar, A. Bhardwaj and B. Basu, *ACS Appl. Mater. Interfaces*, 2023, **15**(1), 281–291.
16 A. Parihar, N. K. Choudhary and P. Sharma, *Mater. Today Chem.*, 2023, **30**, 101499.

17 L. Jiang, L. Yuan, S. Gao, Y. Y. Xiang, F. Song, W. S. Ma, J. Wan, X. L. Ji and Y. J. Tu, *Anal. Methods*, 2023, **15**(19), 2376–2381.
18 Y. L. Bai, J. J. Zhao, S. L. Wang, T. R. Lin, F. G. Ye and S. L. Zhao, *ACS Appl. Mater. Interfaces*, 2021, **13**(30), 35365–35375.
19 W. Chen and P. Liu, *Adv. Powder Technol.*, 2022, **33**(11), 103816.
20 N. A. Tran, N. T. Hien and N. M. Hoang, *Desalination*, 2023, **548**(116285), 2–14.
21 L. J. Yue, Y. Y. Wei, J. B. Fan, L. Chen, Q. Li, J. L. Du, S. P. Yu and Y. Z. Yang, *New Carbon Mater.*, 2021, **36**(2), 373–389.
22 Y. Zhang, Z. Y. Gao, X. Yang, G. Q. Yang, J. L. Chang and K. Jiang, *RSC Adv.*, 2019, **9**, 6084–6093.
23 G. Kaur, M. Chaudhary, K. C. Jena and N. Singh, *New J. Chem.*, 2020, **44**(25), 10536–10544.
24 N. Sivaraman, V. Duraisamy, L. Lucious, B. Saraswathyamma, S. M. S. Kumar and R. Thangamuthu, *Electrochim. Acta*, 2023, **441**, 141773.
25 L. Wu, X. Y. Shi, P. Das and Z. S. Wu, *Sci. China Mater.*, 2023, **66**, 1702–1718.
26 Z. Y. Guo, Z. L. Wang, Y. G. Liu, H. Wu, Q. Y. Zhang, J. Han, J. N. Liu and C. P. Zhang, *ACS Appl. Mater. Interface*, 2023, **15**(17), 20726–20741.
27 C. A. Ma, C. S. Yin, Y. J. Fan, X. F. Yang and X. P. Zhou, *J. Mater. Sci.*, 2019, **54**(13), 9372–9384.
28 K. L. Qi, R. Y. Lei, F. Zhang and Y. Z. Luo, *Mater. Lett.*, 2023, **331**(15), 1–5.
29 D. Qin, X. G. You and S. C. Bi, *Chem. Eng. J.*, 2022, **428**(1), 131102.
30 M. Vasek, A. T. Souza, T. Allan, J. Kubecka, P. Znachor and J. Hejzlar, *Sci. Total Environ.*, 2021, **755**(Pt. 2), 142550.
31 T. C. Nguyen, D. M. T. Tran, T. D. Hoang, T. L. Le, T. D. Nguyen, T. C. Q. Ngo, T. H. Pham, T. T. L. Vu, V. M. Can and H. Thai, *Polym. Int.*, 2022, **71**(8), 1039–1050.
32 C. Xu, X. Xiao, C. Cai, Q. Cheng, L. Zhu, J. Zhang, B. Wei and H. Wang, *Environ. Sci. Pollut. Res.*, 2023, **30**(19), 54616–54627.
33 Y. Zhang, Z. Y. Gao, X. Yang, J. L. Chang, Z. Y. Liu and K. Jiang, *RSC Adv.*, 2019, **9**(2), 940–949.
34 H. Liu, Y. Zhang, J. H. LIU, P. Hou, J. Zhou and C. Z. Huang, *RSC Adv.*, 2017, **7**(80), 50584–50590.
35 M. Saikia, T. Das and B. K. Saikia, *New J. Chem.*, 2022, **46**(1), 309–321.
36 R. Shakiba-Marani and H. Ehtesabi, *Int. J. Biol. Macromol.*, 2023, **224**, 831–839.
37 H. B. Xu, S. H. Zhou, L. L. Xiao, H. H. Wang, S. Z. Lia and Q. H. Yuan, *J. Mater. Chem. C*, 2015, **3**, 291–297.
38 S. Liu, J. Q. Tian, L. Wang, Y. W. Zhang, X. Y. Qin, Y. L. Luo, A. M. Asiri, A. O. Al-Youbi and X. P. Sun, *Adv. Mater.*, 2012, **24**(15), 2037–2041.
39 M. B. Wu, Y. Wang, W. T. Wu, C. Hu, X. N. Wang, J. T. Zheng, Z. T. Li, B. Jiang and J. S. Qiu, *Carbon*, 2014, **78**, 480–489.
40 M. Sevilla and A. B. Fuertes, *Chemistry*, 2009, **15**(16), 4195–4203.
41 P. J. S. Rana, P. Singh and P. Kar, *J. Mater. Chem. B*, 2016, **4**(35), 5929–5937.
42 J. Manioudakis, F. Victoria, C. A. Thompson, L. Brown, M. Movsum, R. Lucifero and R. Naccache, *J. Mater. Chem. C*, 2019, **7**(4), 853–862.
43 R. Tabaraki and Z. Rahmatinya, *J. Fluoresc.*, 2021, **31**, 881–887.
44 S. Ding, Y. Gao, B. S. Ni and X. D. Yang, *Inorg. Chem. Commun.*, 2021, **130**, 108636–108641.
45 M. Moniruzzaman and J. S. Kim, *Nanoscale*, 2023, **15**(34), 13858–13885.
46 X. J. Yang, Y. Y. Wang, J. J. Xu and M. X. Zhao, *Microchem. J.*, 2021, **165**, 106033.
47 X. C. Li, Q. Hu, K. Yang, S. J. Zhao, S. H. Zhu, B. H. Wang, Y. Zhang, J. N. Yi, X. Z. Song and M. H. Lan, *Sens. Actuators, B*, 2022, **371**, 132534.
48 W. L. Gao, H. H. Song, X. Wang, X. Q. Liu, X. B. Pang, Y. M. Zhou and X. J. Peng, *ACS Appl. Mater. Interfaces*, 2018, **10**(1), 1147–1154.
49 Q. Tan, X. Y. Li, P. Sun, J. Zhao, Q. Y. Yang, L. M. Wang, Y. Deng and G. Q. Shen, *Anal. Methods*, 2022, **14**(36), 3573–3582.
50 G. Ning, B. Li, J. J. Liu, Q. Xiao and S. Huang, *Anal. Bioanal. Chem.*, 2022, **414**(6), 2219–2233.
51 Y. Luo, C. Cui, X. Zhang, Y. Jiang, Z. Xiang, C. Ji and Z. Peng, *Molecules*, 2023, **28**(4), 1566.
52 S. Liao, X. Zhao, F. Zhu, M. Chen, Z. Wu, X. Song, H. Yang and X. Chen, *Talanta*, 2018, **180**, 300–308.
53 L. Zhao, Y. Bai, Y. Wen and X. Yang, *Anal. Methods*, 2022, **14**(42), 4230–4235.
54 Y. Wang, J. Lu, L. H. Tang, H. X. Chang and J. H. Li, *Anal. Chem.*, 2009, **81**(23), 9710–9715.
55 C. Xu, H. D. Li and B. Z. Yin, *Biosens. Bioelectron.*, 2015, **72**, 275–281.
56 Z. Q. Song, F. Y. Quan, Y. H. Xu, M. L. Liu, L. Cui and J. Q. Liu, *Carbon*, 2016, **104**, 169–178.
57 H. Y. Zou, T. Yang, J. Lan and C. Z. Huang, *Anal. Methods*, 2017, **9**(5), 841–846.